

Received June 14, 2020, accepted June 29, 2020, date of publication July 2, 2020, date of current version July 23, 2020.

Digital Object Identifier 10.1109/ACCESS.2020.3006627

A Real-Time Phase Center Variation Compensation Algorithm for the Anti-Jamming GNSS Antennas

KEJIN CAO¹, LEI WANG^{1,2}, (Member, IEEE), BAO LI¹, AND HENGCHAO MA¹

¹College of Electronic Science, Naval University of Engineering, Wuhan 430070, China

²State Key Laboratory of Information Engineering in Surveying, Mapping and Remote Sensing, Wuhan University, Wuhan 430079, China

Corresponding author: Lei Wang (lei.wang@whu.edu.cn)


This work was supported in part by the National Natural Science Foundation of China (NSFC) under Grant 41704002 and Grant 41631072, and in part by the Fundamental Research Funds for the Central Universities.

ABSTRACT The anti-jamming antenna is one of the most efficient ways to resist the adversary effect of the interference signal in GNSS positioning. Most anti-jamming antennas can adaptively adjust the radiation figure of the antenna to minimize the interference impact. A side effect of changing the radiation figure is that the antenna phase center (APC) is also changed accordingly. Meanwhile, a stable phase center is a prerequisite for high precision GNSS positioning, thus the anti-jamming and high-precision becomes a dilemma for the GNSS antenna design. This study proposed an efficient antenna phase center variation (PCV) compensation algorithm for the anti-jamming antennas which enables real-time high-precision applications with the anti-jamming antennas. The performance of the algorithm is evaluated with the short baseline tests, and the results indicate that the proposed algorithm can reduce the carrier phase residuals by compensation of the anti-jamming antenna PCV and consequently, the 3D root mean squares (RMS) of real-time kinematic (RTK) positioning in two experiments is improved by 42.3% and 9.7% respectively. After PCV correction, the RTK positioning with the anti-jamming antennas achieves better than 4 cm accuracy.

INDEX TERMS Anti-jamming antenna, GNSS antenna, phase center variation, power inversion algorithm, precise positioning.

I. INTRODUCTION

The vulnerability of the navigation signal is one of the major challenges of the global navigation satellite system (GNSS) [1]. Suppressing the harmful signal interference by specially designed GNSS antenna array is the mainstream technique, which is named anti-jamming GNSS antenna. The adaptive array anti-jamming antenna is the main part of the GNSS receiver to suppress the interference signals. With multiple antenna elements, it is possible to change the radiation figure of the antenna to resist the signal interferences [2]. There have been a few researchers achieved outstanding anti-jamming performance with the antenna array technique. The performance of the anti-jamming can be measured by the capacity of resisting jamming-to-signal ratio (JSR). One of the side effects of changing the antenna radiation figure is that the phase center of the antenna also changed accordingly, which lead adversary effect on the GNSS precise positioning.

The associate editor coordinating the review of this manuscript and approving it for publication was Venkata Ratnam Devanaboyina .

Kim pointed out that the controlled reception pattern antenna array (CRPAs) produces phase deviation after using an adaptive algorithm [3] in 2005 and the deviation is related to the weights of the antenna array. The phase center of the GNSS antenna may change up to a few decimeters in extreme cases which have a significant impact on the positioning precision. As a result, the precise positioning antenna and anti-jamming antenna become a dilemma in the GNSS antenna design [4].

There have been a few researchers engaged to solve the phase center stability problem of the anti-jamming antennas, and substantial progress has been made. For example, Konovaltsev *et al.* pointed out that millimeter level phase center stability is achievable with precisely modeling the radiation field of each array element and the transmission characteristics of the RF front-end [5]. This method is theoretically rigorous but less practical. Zhao *et al.* revealed the impact of beamforming on the code biases reaches a few decimeters by simulation [4]. Wang *et al.* further confirmed the phase center variation of anti-jamming antenna reaches a few centimeters [6]. Chen *et al.* analyzed the phase center

variation characteristic using a two-element antenna array [7]. Gupta discussed the availability, accuracy, and integrity of the GNSS adaptive array antenna technology and he gave a cross-correlation peak expression of phase deviation [8]. Unfortunately, the computation efficiency of the method is unsatisfactory. Liu et. al examined the impact of the element geometry configuration on the phase center variation [9]. Li *et al.* evaluated the performance of the phase centers for the four-element antenna array from an array selection perspective [10]. Cao *et al.* analyzed the space-time anti-jamming algorithm and proposed a signal processing algorithm of satellite navigation unbiased anti-jamming array, which makes the code phase deviation constant [11]. Chen proposed a space-time anti-jamming algorithm under unbiased constraint, which has linear phase characteristics and does not introduce carrier phase variation. The performance of the algorithm is close to the minimum variance distortionless response (MVDR) algorithm [12], [13], but the algorithm is too complex to implement in the resources constrained environment. Whether the carrier phase measurement meets the high-precision application mainly depends on the disturbance amplitude and phase center of the array element for the symmetrical antenna array using the power inversion (PI) algorithm [14]. It is a promising clue that compensating the phase center of the antenna array efficiently is possible.

To meet the anti-jamming and high-precision requirements simultaneously, this study analyzed the relationship between the signal incidence angle and the phase error of the array antenna. Consequently, we can compensate for the phase error of the array antenna caused by the radiation change in real-time mode. After the phase error is compensated, a stable phase center can be expected for the anti-jamming antennas. Compared to the MVDR algorithm, the proposed method needs neither linear constraint nor special requirements of the receiver structure. The proposed algorithm is also computational efficient so that it can be implemented on resources constrained environment and reduce the hardware cost for precise positioning type, anti-jamming GNSS antennas. We also tested our algorithm with the field RTK experiments, which confirmed the effectiveness of our algorithm.

II. THE PCV COMPENSATION ALGORITHM FOR THE ANTI-JAMMING GNSS ANTENNA

For the GNSS positioning applications, the position of users can be determined by measuring the distance between the GNSS satellite and user antenna from GNSS ranging signals. More specifically, the ‘distance’ refers to the difference between the antenna phase center of the satellite and the receiver. The designed phase center is stable relative to the geometrical center of the antenna and it generally depends on the antenna design. This designed antenna phase center is known as the antenna phase center (APC) [15]. In reality, the carrier phase measured by the GNSS receiver is often referred to as the instantaneous phase center (IPC), which depends on the signal incoming direction. Due to the imperfection of the GNSS antenna implementation, the IPC is nor-

mally different from the APC and the difference between the IPC and APC is known as the antenna phase center variation (PCV). The antenna PCV depends on the antenna design, which varies between millimeter to meter level. The PCV impact is satellite-dependent, so a large PCV will degrade the positioning accuracy, so it is always considered as an error source in GNSS precise positioning applications [16]. For example, the geodetic level GNSS antenna normally has its PCV smaller than a few millimeters [17], [18].

A standard GNSS antenna does not change its radiation figure, so its PCV can be calibrated with long term observations. For the anti-jamming antennas, the receiver antenna involves multiple individual antenna elements and the radiation figures are adjustable according to the interference signal direction, hence its PCV also changed with the radiation figure. It cannot be directly calibrated, so it is more challenging to handle the PCV error of the anti-jamming antenna.

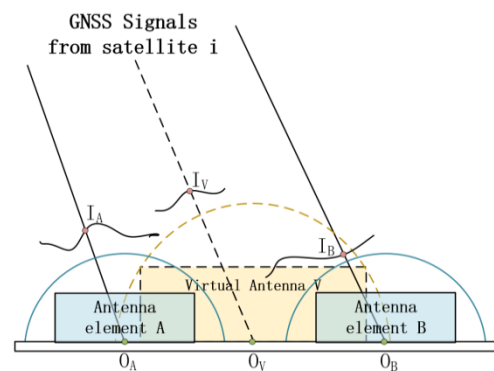


FIGURE 1. Antenna phase center model for the anti-jamming GNSS antenna.

A. PHASE CENTER MODEL FOR THE ANTI-JAMMING GNSS ANTENNAS

In this study, we attempt to compensate the PCV error for the anti-jamming antenna. At first, we need to introduce the antenna phase model of the anti-jamming antenna. The anti-jamming GNSS antenna often consists of multiple antenna elements. These antenna elements form a virtual antenna. Then, the radiation figure of the virtual antenna can be changed by adjusting the weight of each antenna element. The antenna phase center model for the anti-jamming antenna can be illustrated in Figure 1. In the figure, the whole anti-jamming antenna consists of two antenna elements. The APC of each antenna element is denoted as O_A and O_B , the IPCs of the two antenna elements for the satellite i denote as I_A and I_B . The formed virtual antenna is denoted as V . The APC and IPC of the virtual antenna are denoted as O_V and I_V , The difference between O_V and I_V are the PCV of the virtual antenna. Since the radiation figure of the virtual antenna is changed according to the interference signal, the PCV also varies accordingly. Compensating the PCV for the anti-jamming antenna is to remove the PCV error of the virtual antenna V .

The proposed anti-jamming antenna PCV compensation algorithm involves four steps and the flowchart of the algorithm is illustrated in Figure 2. The purpose of the algorithm is to enable the anti-jamming and high-precision simultaneously, so the first two steps are implementing the anti-jamming function and the last two steps are designed for antenna PCV compensation.

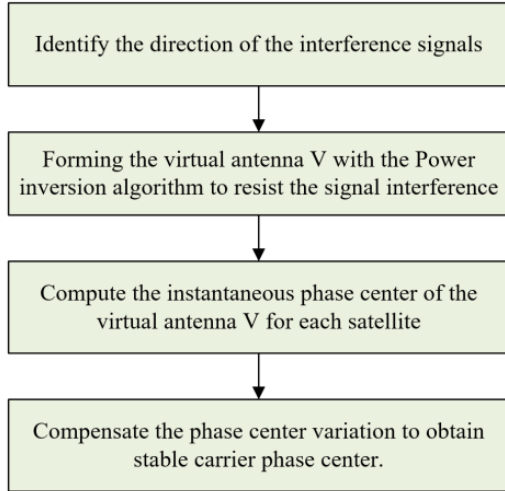


FIGURE 2. The procedure of PCV compensation for the anti-jamming antennas.

B. BEAMFORMING WITH THE POWER INVERSION ALGORITHM

There are a few anti-jamming algorithms with the adaptive antenna array, such as the least mean-square (LMS), recursive least-squares (RLS), simple matrix inversion (SMI) [19], uniform linear array(ULA), space-time adaptive processing (STAP) *et al.* [20]. Different algorithms have different anti-jamming performance and require different inputs [21]. In this study, we use the power inversion (PI) algorithm to form the nulling notch, which does not need prior interference information [22]. The principle of the PI algorithm can be described as follows.

For an antenna array with n elements, the signal received by the i th elements is denoted as $x_i(t)$, then the input signals of the antenna array can be expressed as a vector, denoted as $\mathbf{x}(n) = [x_1(n), x_2(n), \dots, x_N(n)]^T$. The PI algorithm adjusts the weight factor of each element dynamically to change the radiation figure of the virtual antenna. The weight factor of the i th element is denoted as w_i then the weight vector of the array antenna can be written as $\mathbf{w} = [w_1, w_2, \dots, w_N]^T$. The output of the antenna array can be expressed as [14]:

$$y(n) = \mathbf{w}^T \mathbf{x}(n) \quad (1)$$

where $y(n)$ is the output of the antenna array. The superscript T means transpose of the matrix

The optimization objective of the PI algorithm is to minimize the output power of the adaptive array antenna [14]:

$$\begin{cases} \text{Min} \{P_{out} = E [|y(n)|^2] \} \\ \mathbf{w}^T \mathbf{s} = 1 \end{cases} \quad (2)$$

To ensure that the weight vector is not a zero vector, set the constraint condition $\mathbf{w}^T \mathbf{s} = 1$, where \mathbf{s} represents the reference vector, and its weight coefficient is always 1. For example, the first matrix element can be used as the reference matrix element, $\mathbf{s} = [1, 0, \dots, 0]^T$. Because the interference signal is usually stronger than the real signal, and the objective of the optimization is to make the antenna pattern forming a nulling notch in the interference signal incoming direction to suppress the adversary impact of interference signals. The stronger the interference signal, the deeper the zero notches [23], [24], The specific implementation of the algorithm is shown in Figure 3. In the PI algorithm, the direction of the jamming signals can be automatically determined, so no extra action is required to calculate the interference signal direction.

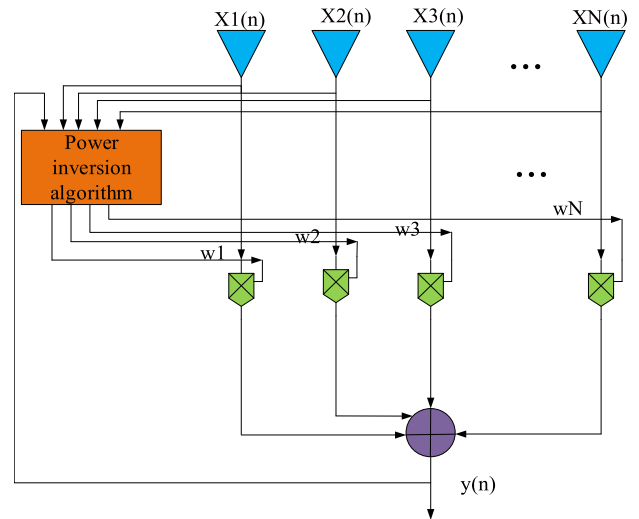


FIGURE 3. The system diagram of the power inverted n -element array model.

The output power of the array P_{out} can be expressed as:

$$P_{out} = E [|y(n)|^2] = \mathbf{w}^T \mathbf{R}_{xx} \mathbf{w} \quad (3)$$

where $\mathbf{R}_{xx} = E [\mathbf{x}(n) \mathbf{x}^T(n)]$ is the autocorrelation matrix of the input vector $\mathbf{x}(n)$. The constrained optimizing problem can be solved with the Lagrange multiplier algorithm. The Lagrange function can be written as:

$$L(\mathbf{w}) = \mathbf{w}^T \mathbf{R}_{xx} \mathbf{w} + \gamma (\mathbf{w}^T \mathbf{s} - 1) \quad (4)$$

where γ is the coefficient of Lagrange multiplier. Given the gradient of the Lagrange function follows $\nabla_{\mathbf{w}} L(\mathbf{w}) = 0$, then, the solution of the optimal weight vector is:

$$\mathbf{w}_{opt} = P_{out \min} \mathbf{R}_{xx}^{-1} \mathbf{s} \quad (5)$$

where $P_{out \min} = (\mathbf{s}^T \mathbf{R}_{xx}^{-1} \mathbf{s})^{-1}$ is the minimal output power.

For example, the Beidou navigation satellite signal can be expressed as:

$$S^i(t) = aC^i(t)D^i(t)\cos(\theta t + \varphi^i) \quad (6)$$

where i is the satellite number, a is the signal amplitude; $C^i(t)$ is the signal ranging code; $D^i(t)$ is the data code modulated on the signal ranging code; θ is the signal carrier frequency; φ^i is the initial phase of the signal carrier. According to the Euler equation, the signal $S^i(t)$ can also be expressed as:

$$S^i(t) = M^i(e^{j(\theta t + \varphi)} + e^{-j(\theta t + \varphi)}) \quad (7)$$

where $M^i = aC^i(t)D^i(t)$ is the amplitude of the signal. The PI algorithm makes $E[|y(n)|^2]$ minimum, where $|y(n)|$ is the amplitude. It is clear that the PI algorithm only considers the amplitude of the signal M but the variation of the phase φ in $S^i(t)$ is not considered. When the interference signal introduced, the weight coefficient changes and the phase φ will change dynamically with the signal strength, direction, and the number of the interference signal, which leads the phase of the signal changed. The distorted signal can be expressed as:

$$S^i(t) = |H(s)| (e^{(\theta t + \varphi_i)j} + e^{-(\theta t + \varphi_i)j}) \quad (8)$$

where $|H(s)|$ is the amplitude of GNSS signal, φ_i is the distorted phase of the signal, set $\phi = \varphi_i - \varphi$, ϕ is the phase center error caused by the beamforming procedure.

C. MODELING THE PHASE CENTER OF THE NULLING ANTENNA ARRAY

As stated, the phase center error is introduced during the beamforming procedure, which dynamically changed as the interference signals. On the other hand, precise positioning applications require a stable antenna phase center. In this study, we attempt to model the phase center error during the beamforming so that the phase center error can be compensated in real-time.

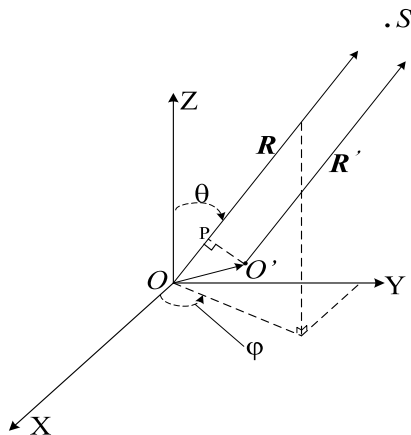


FIGURE 4. The effect of the phase center drift on the signal phase.

The first step is to model the phase center of the nulling antenna array. The effect of the phase center variation affects

the measured signal phase. The geometrical relationship can be illustrated in figure 4. Given one antenna element phase center located at the origin O , a navigation satellite signal S comes from the direction (θ, φ) , where θ and φ are the zenith angle and the azimuth angle respectively. The carrier phase of the signal S at the O point can be expressed as $\psi_0(\theta, \varphi)$. If the phase center of the antenna element is shifted to O' (x_0, y_0, z_0), the observed phase can be expressed as:

$$\psi'(\theta, \varphi) = \psi_0(\theta, \varphi) - \frac{2\pi}{\lambda} |OP| \quad (9)$$

If $\vec{r} = (\sin \theta \cos \varphi, \sin \theta \sin \varphi, \cos \theta)$, so $|OP| = \vec{OO}' \cdot \frac{\vec{OP}}{|OP|} = \vec{OO}' \cdot \vec{r}$. According to the reciprocity theorem, the phase of the signal S relative to the phase center O' can be denoted as $\psi'(\theta, \varphi)$. Assuming the far-field radiation pattern function of the array antenna at the origin can be expressed as:

$$f_0(\theta, \varphi) = A_0(\theta, \varphi) e^{i\psi_0(\theta, \varphi)} \quad (10)$$

where $A_0(\theta, \varphi)$ is the real amplitude value. Since $|OP|$ is far less than $|\vec{R}'|$, then the amplitude value at O' can be approximated as $A_0(\theta, \varphi)$, and the far-field radiation pattern function can be given as:

$$f_{O'}(\theta, \varphi) = A_0(\theta, \varphi) e^{i[\psi_0(\theta, \varphi) - k\vec{OO}' \cdot \vec{r}]} \quad (11)$$

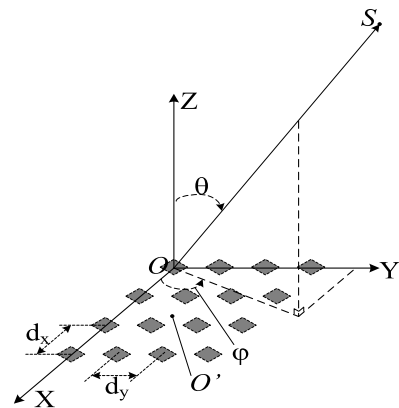


FIGURE 5. Two-dimensional array antenna mode.

For the N element antenna array with multiple element case. A two-dimensional GNSS antenna array composed with N identical ideal array elements is illustrated in figure 5. All these elements are assumed installed on the same plane. The inter-elements space between adjacent elements is denoted as dx and dy in ox axis direction and oy axis direction respectively. For the GNSS antenna array composed of N identical ideal elements, the antenna coordinates of any element are denoted as $F_n(x_n, y_n, z_n)$ ($n = 1, 2, \dots, N$), without considering the mutual coupling effect between elements. If the adaptive algorithm is not applicable, its far-field radiation

pattern function (RPF) can be expressed as:

$$f(\theta, \varphi) = \sum_{n=1}^N A_0(\theta, \varphi) e^{i[\psi_0(\theta, \varphi) - k\vec{OF}_n \cdot \vec{r}]} \quad (12)$$

If the weight of the n matrix element is w_n ($n = 1, 2, \dots, N$), taking its conjugate w_n^* , then the far-field radiation pattern function of the array antenna with an adaptive algorithm can be expressed as:

$$f(\theta, \varphi) = A_0(\theta, \varphi) e^{i\psi_0(\theta, \varphi)} \sum_{n=1}^N w_n^* e^{-ik\vec{OF}_n \cdot \vec{r}} \quad (13)$$

If the phase pattern function (PPF) corresponding to the array antenna is $\psi(\theta, \varphi)$, then $f(\theta, \varphi) = Ae^{i\psi(\theta, \varphi)}$, where A is the real function.

D. INSTANTANEOUS PHASE CENTER ESTIMATION

Define the antenna reference point (ARP) as the geometric center of the antenna array, denoted as $O(0,0,0)$, and the far-field phase subject to the ARP is denoted as $\psi(\theta, \varphi)$. Then, the far-field phase error introduced by the phase center $O'(x_0, y_0, z_0)$ can be viewed as a constant, which can be defined as:

$$C = \psi(\theta, \varphi) - k(\vec{OO}' \cdot \vec{r}) \quad (14)$$

where C is the constant phase bias in the satellite incidence angle direction, which can be used to compensate the antenna PCV.

In practice, how to precisely estimate the constant bias C is the real challenge. Considering the far-field wave is a spherical wave, given the sphere center O' , then the phase biases near the satellite can be approximated viewed as C , hence the constant bias for this particular satellite can be estimated from the set of points. According to literature, $\varphi = 0^\circ$ or 90° , the two-dimensional phase center is obtained in the direction of the main radiation lobe of xoy plane and $yozy$ plane respectively, and its mean value is taken as the calculated phase center.

In this study, the point set in the region around the sphere of its far-field are considered, and the phase values are respectively set as $\psi(\theta_i, \varphi_i)$, $i = 1, 2, \dots, n$, $n \geq 4$, then the observation equation can be given as:

$$k(x_0 \sin \theta_i \cos \varphi_i + y_0 \sin \theta_i \sin \varphi_i + z_0 \cos \theta_i) + C = \psi(\theta_i, \varphi_i) \quad (15)$$

For all the points in the set, we form a group of equations:

$$A = \begin{bmatrix} k \sin \theta_1 \cos \varphi_1 & k \sin \theta_1 \sin \varphi_1 & k \cos \theta_1 & 1 \\ k \sin \theta_2 \cos \varphi_2 & k \sin \theta_2 \sin \varphi_2 & k \cos \theta_2 & 1 \\ \vdots & \vdots & \vdots & \vdots \end{bmatrix}, \quad X = \begin{bmatrix} x_0 \\ y_0 \\ z_0 \\ C \end{bmatrix}, \quad y = \begin{bmatrix} \psi(\theta_1, \varphi_1) \\ \psi(\theta_2, \varphi_2) \\ \vdots \end{bmatrix} \quad (16)$$

The observation equation can be simplified as a linear system:

$$AX = y \quad (17)$$

The linear equation can be solved with the least-square estimator, given as:

$$X = (A^T A)^{-1} A^T y \quad (18)$$

As a result, the phase center (x_0, y_0, z_0) is estimated and the phase center error ϕ compensation can be calculated accordingly $d_{OO'.r}$ expressed in the distance unit and $d_{OO'.r}/\lambda$ is in the whole cycle number.

E. COMPENSATING THE PCV BIASES

The solution position of the receiver is eventually derived from the observation equation. The pseudorange and carrier phase observation equations of GNSS can be expressed as [25]:

$$\begin{cases} P_i = \rho + c(\delta t_u - \delta t^s) + I_i + T + \delta_{PCV} + \varepsilon_\rho \\ L_i = \rho + c(\delta t_u - \delta t^s) - I_i + T + \lambda_i N_i + \delta_{PCV} + \varepsilon_\phi \end{cases} \quad (19)$$

where P_i and L_i are pseudorange and carrier phase measurement expressed in the meter. ρ is the distance between the satellite antenna PCO and the receiving antenna PCO. c is the speed of light, δt_u and δt^s are the user receiver clock error and satellite clock error. I_i and T is the ionospheric delay on i th frequency and tropospheric delay respectively. λ_i and N_i are the wavelength and the carrier phase ambiguity of i th frequency respectively, ε_ρ and ε_ϕ are pseudorange and carrier phase measurement noise. δ_{PCV} is the phase error of the receiver antenna array. For the anti-jamming antennas, the receiving antenna PCO is changed, so the variation of PCO has to be compensated to meet the precise positioning requirement. In our approach, δ_{PCV} can be calculated according to the weighting factors in the PI algorithm and satellite incidence angle, and then used to compensate them in pseudorange and carrier phase measurement. After PCV compensated, the anti-jamming antenna virtual gains a stable carrier phase center and capacity to support precise positioning applications. The flowchart of the PCV compensation procedure is shown in Figure 6. The PCV compensation algorithm is computationally efficient, so it can be implemented in real-time.

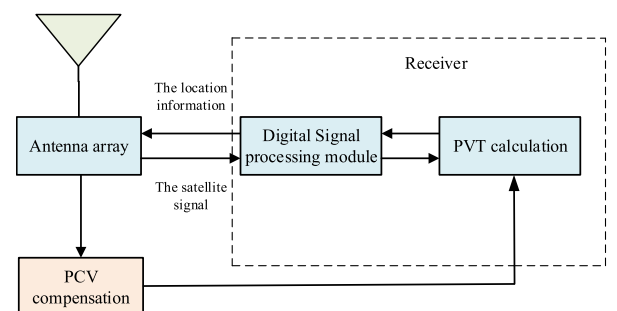


FIGURE 6. PCV compensation procedure.

III. IMPACT OF THE INTERFERENCES ON THE ANTENNA PCV

The impact of the phase variation in beamforming can be examined with the numerical simulation. In this study, we focus on a 1×2 or 2×2 antenna array. Theoretically, a two-element antenna can produce one nulling notch and The 4 element antenna can resist up to 3 interference signals from different directions at maximum. In the simulation, we assume there is one or more interference signal presence, and then compute the weight factors according to the PI algorithm. After that, the radiation figure change, and the phase distortion is examined to unveil the impact of beamforming. In this study, we checked the interference impact on the Beidou B1I signal, whose center frequency is 1561.098 MHz. The array element spacing is half of the signal wavelength and we assume the antenna array suffers from uncorrelated narrow-band interference. The jamming-to-signal ratio was 30dB. The discussion considers the single interference scenario and multiple interference scenarios.

A. SINGLE INTERFERENCE SCENARIOS

At first, we examined the impact of different interferences direction and interference signal strength for the single interference scenario and the results are presented in Figure 7 and Figure 8.

The radiation figure of the four-element antenna array under different interference scenarios is presented in Figure 7. The figure indicated that the gain of the antenna array is changed according to the interference signal incidence angle. The antenna forms nulling notch to minimize the interference impact. The gain in a certain direction reaches about -40 dB. The adaptive antenna may work well when the jamming-to-signal ratio (JSR) is within a certain extent.

The impact of the beamforming on the received signal phase is illustrated in Figure 8. The figure indicates that the impact of the beamforming on the received signal phase may larger than 1 cycles, which is corresponding to a few decimeter level PCV errors, hence it has to be considered for the centimeter-level precise positioning. Generally, the phase abnormal caused by the interference is around the interference direction and the opposite interference direction. Sometimes the PCV error causes phase discontinuity.

B. MULTIPLE INTERFERENCE SCENARIO

It can be seen from the simulation that in the direction where the antenna gain changes, the phase that needs to be compensated also changes dramatically, and even abrupt phase inversion occurs, which indicates that a sudden phase change may occur even the satellite moves continuously. Without compensation, it will cause the receiver to lose carrier phase signal tracking. We examined the situation of three interferences, and set the interference directions to $(40^\circ, 10^\circ)$, $(30^\circ, 70^\circ)$, $(60^\circ, 130^\circ)$, and still choose the same four satellite directions and interference. The ratio is calculated, and the antenna gain direction and phase compensation are

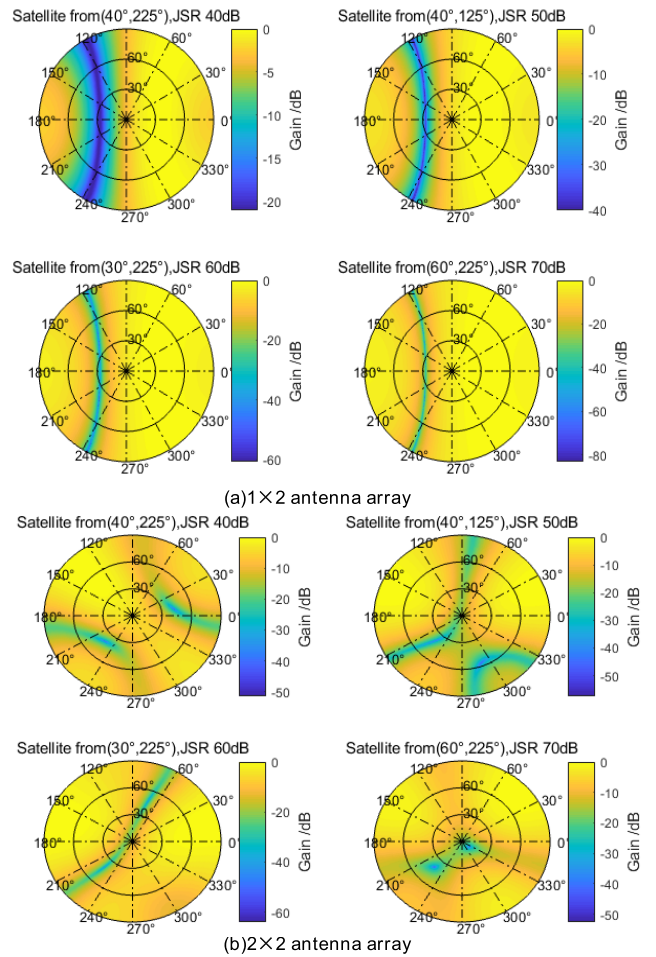


FIGURE 7. The radiation figure of the antenna array under single interference scenario.

obtained as shown in Figure 9 and Figure 10. Similarly, In three interferences case, the antenna pattern also has an abrupt phase change near the zero-pitched azimuth.

We examined the jamming signal power impact on the antenna phase variation and the results are presented in Figure 11. The figure reveals the phase center variation on different zenith angle and azimuth angle under different JSR. With a given jamming signal from the direction $(40^\circ, 225^\circ)$, the carrier phase variation is continuous in a weak jamming signal scenario, but a phase jump occurs as the jamming signal power increases. For the JSR higher than 60 dB case, the IPC does not change anymore.

It can be seen more clearly from this figure that a 180° phase change occurs near the zero notches. In addition to the interference direction, the gain nulls also appear in the non-interference direction and causing unnecessary signal loss, which is one of the reasons why the array antenna cannot perform high-precision positioning.

IV. PCV COMPENSATION PERFORMANCE EVALUATION

In order to evaluate the PCV compensation algorithm, we carried out the field experiment and the results are discussed in this section.

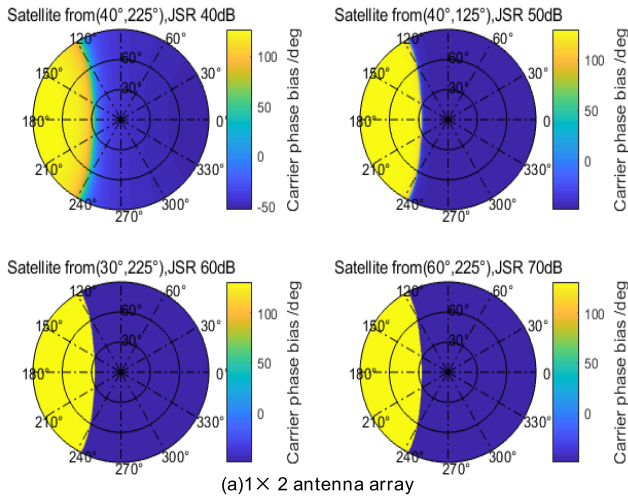


FIGURE 8. The impact of the beamforming on the received signal phase under a single interference scenario.

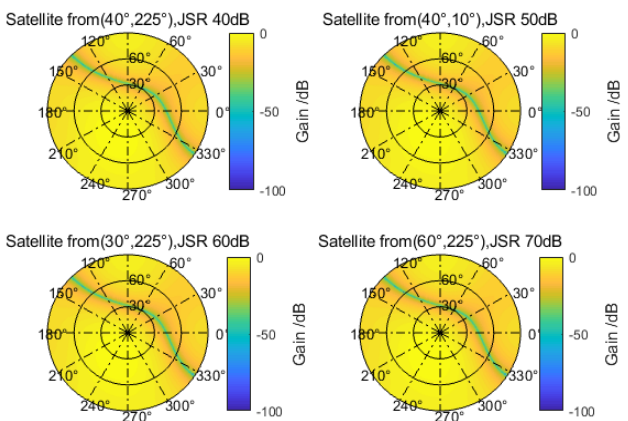


FIGURE 9. The radiation figure of the antenna array under three interference scenarios.

A. EXPERIMENT SETUPS

Since the antenna PCV is lumped with other biases in GNSS measurements, so it is difficult to isolate the antenna PCV effect directly. In this study, we use the short baseline RTK (real-time kinematic) data processing to isolate the PCV biases. For the short-baseline RTK scenario, the double dif-

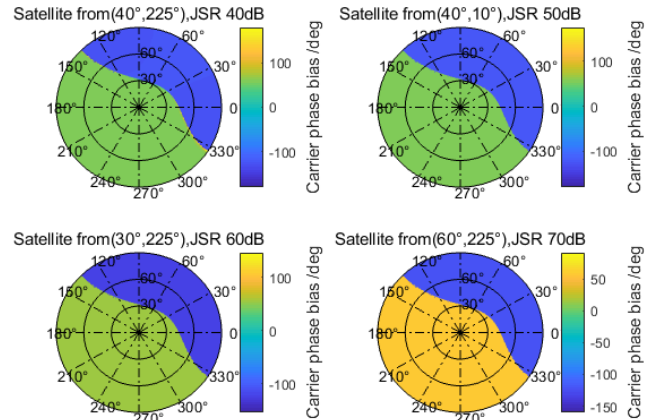


FIGURE 10. The impact of the beamforming on the received signal phase under three interference scenarios.

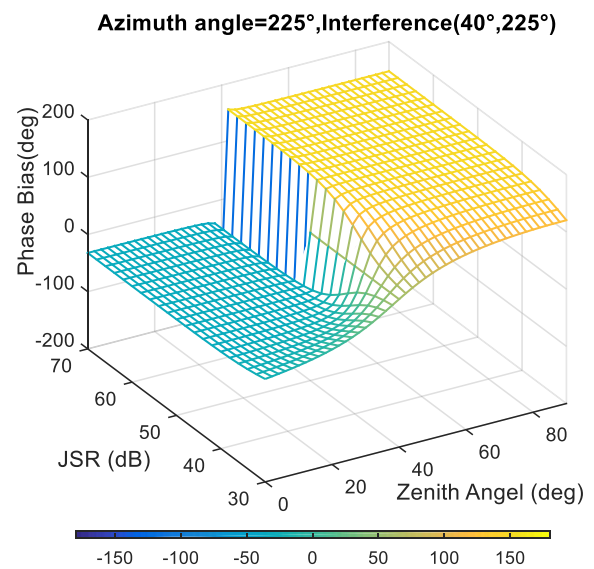
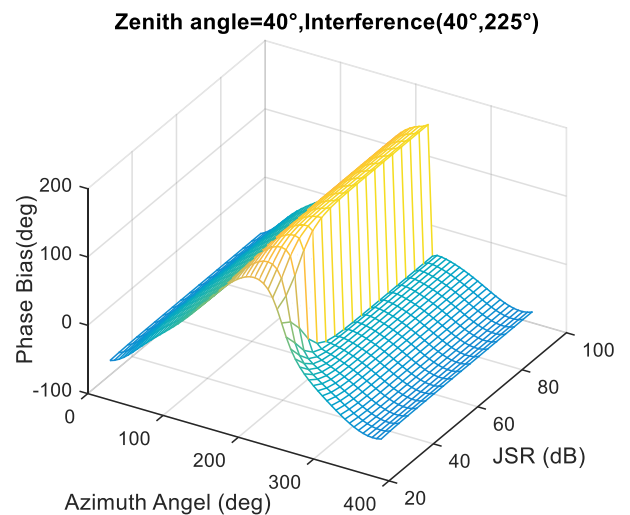


FIGURE 11. Phase error compensation of azimuth and altitude.

ferenced observations can be expressed as [26]:

$$\begin{cases} \Delta \nabla P_i = \Delta \nabla \rho + \Delta \nabla \delta_{PCV} + \Delta \nabla \varepsilon_\rho \\ \Delta \nabla L_i = \Delta \nabla \rho + \lambda_i \Delta \nabla N_i + \Delta \nabla \delta_{PCV} + \Delta \nabla \varepsilon_\phi \end{cases} \quad (20)$$

where $\Delta\nabla$ is the double-differenced operator. The equation indicates that the short-baseline RTK cancels out most errors in the GNSS observations and the remained biases are the double-differenced geometry distance, antenna PCV bias, and double-differenced carrier phase ambiguity and receiver noise. For the normal geodetic grade GNSS antenna, the PCV bias is fairly small, which is normally at millimeter-level, but it becomes non-negligible for the anti-jamming antenna. If the antenna phase center (APC) of the reference and rover antennas are precisely known, then the geometry term can be further removed. The carrier phase measurement has millimeter level measurement noise, so it can be neglected. Although the true value of the double-differenced carrier phase ambiguity is unknown, it is given as integer constant unless cycle slips occur. If the carrier phase ambiguity is correctly fixed to the right integer, the remaining biases can be considered as the double-differenced PCV biases. In our experiment, the PCV impact of the reference antenna is negligible, since the geodetic grade GNSS antenna has fairly stable PCV. Hence, the remaining biases in the double differenced observations can be viewed as the single-differenced PCV bias from the anti-jamming antenna.

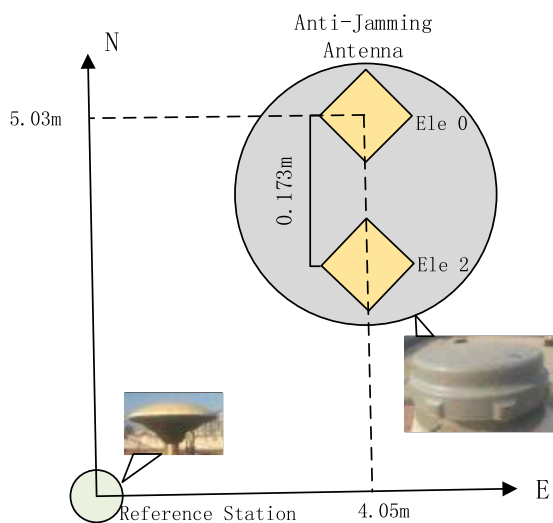


FIGURE 12. Experiment setup of the GNSS RTK testbed.

The experiment setup is illustrated in Figure 12. We deployed two sets of GNSS antennas on fixed points and one of them is an anti-jamming antenna array with two elements. The antenna deployed on the reference station is a commercial GNSS antenna without an anti-jamming function. The anti-jamming antenna array can form the nulling with the power inversion algorithm introduced in section 2.2 and then reconstruct the radio frequency signals, so that the antenna can work with the commercial GNSS receivers. In this study, two commercial GNSS boards named ComNav K508 are used for tracking GNSS signals. Both antennas are capable of tracking B3 signals from the Beidou system with center frequency 1268.52 MHz.

The key point of our experiment is determining the reference APC of the anti-jamming antenna array. The experiment follows a two-step procedure: (1) Compute the theoretical PCV of the anti-jamming antenna array. (2) Evaluating the PCV biases compensation performance with the short baseline RTK algorithm.

B. ESTIMATING THE MEAN APC OF THE ANTENNA ARRAY

The antenna phase center (APC) of the antenna array cannot be measured directly, since it is invisible. Therefore, we use a two-step procedure to precisely determine the APC of the anti-jamming antenna. Firstly, we employ the RTK algorithm to precisely determine the APC of each element in the array. In this step, we circumvent the anti-jamming module in the antenna array, so the antenna elements served as a normal GNSS antenna. In this way, the short-baseline RTK achieves millimeter level positioning accuracy. Then, we find the middle point of the two elements and fixed it as the APC of the antenna array. Although this method is not theoretically rigorous, it achieves an acceptable accuracy. The RTK positioning results of the two elements in the antenna array are presented in Figure 13. The figure indicates that short-baseline RTK is capable of determining the APC of each element at the millimeter level. The distance between the physical centers of the two elements is 220 mm, while the distance between the two APC is 173.7 mm from RTK solution, which means APC does not coincide with the physical center of the element. We computed the baseline length between the reference antenna and the elements 0 and elements 2 are 6.459 m and 6.303 m. Then, the theoretical APC of the antenna array is considered as the middle point of the two APCs and the baseline length is 6.381 m. In order to check the correctness of the APC, we also measured the distance between the physical centers of the two antennas with a band tape, which gives a distance of 6.35 m. The band-tape can only measure the distance from the outside of the antenna, which is different from the true APC of the two antennas. But the RTK solution still achieves highly coincide with the results from band tape, so we consider the APC of the antenna array estimated from RTK is reliable.

C. PCV CORRECTION PERFORMANCE EVALUATION

With the reference APC determined, the PCV bias can be isolated with RTK ambiguity fixed to an integer. Before calibrating the PCV of the anti-jamming antenna, the carrier phase residuals of the short baseline RTK with a standard GNSS antenna should be examined. We fixed the coordinates of the two elements to their reference coordinates and examine the carrier phase residuals. For the short-baseline RTK, the success rate of the carrier phase ambiguity resolution is almost 100%, so the carrier phase residuals follow the normal distribution. The carrier phase residuals distribution and fitted probability density function (PDF) of the two elements are presented in Figure 14. The figure indicates that the carrier phase residuals follow the normal distribution with a standard deviation of 7.8 mm and 6.5 mm respectively. The mean value of the carrier phase residuals is smaller than 1 mm, which can

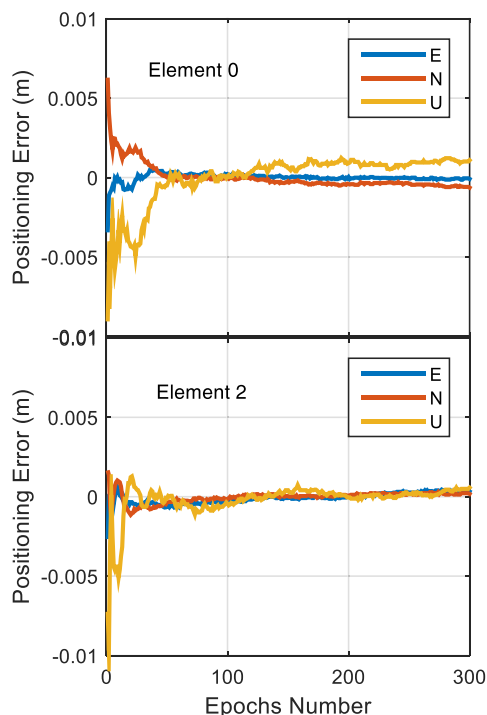


FIGURE 13. RTK Positioning error without the anti-jamming module (Upper: Element 0, Lower: Element 2).

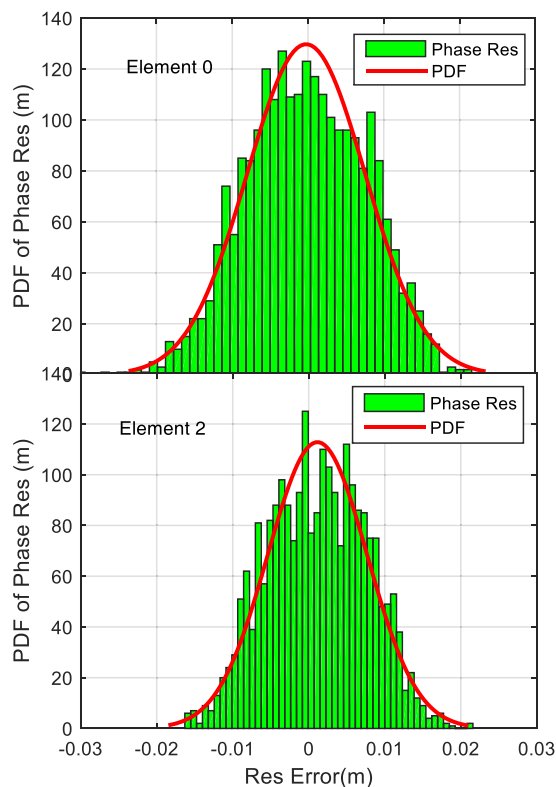


FIGURE 14. The carrier phase residuals of the short-baseline RTK without the anti-jamming module.

be neglected. Hence, the PCV impact on the standard GNSS antenna for the short baseline is limited.

With elements in the anti-jamming antenna well tested, we start evaluated the phase center variation in the anti-

jamming mode. In order to evaluate the performance of the PCV compensation algorithms, we carried out two tests with different weights on the two elements. In the current stage, we used fixed weight to control the uncertainty caused by the weight fluctuation. As analyzed, two elements of the antenna array are able to produce one nulling point. The experiments were carried on 4th June 2020 and the sky plot of the Beidou satellites are illustrated in Figure 15. The elements 0 is used as the reference elements with its weight always equals to 1. The weight of element 2 is set as 0.4 and 0.8 respectively in the two experiments.

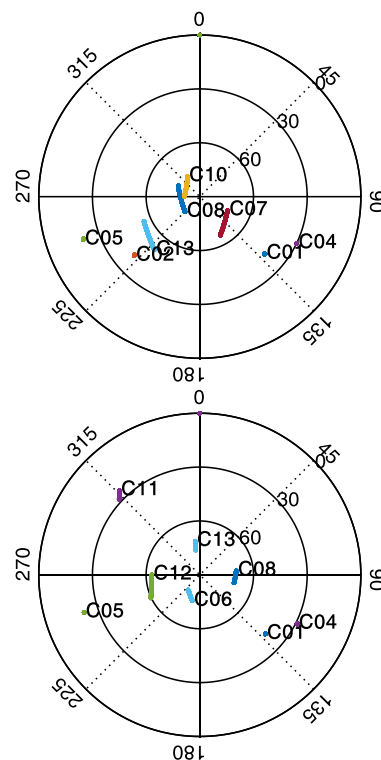


FIGURE 15. The sky plot of Beidou satellite during the two experiments (Upper: Weight 0.4 Lower: Weight 0.8).

The impact of PCV bias on the RTK positioning can be inspected by examining the carrier phase residuals of the RTK fixed solution. In our experiment, we fixed the PCV of the anti-jamming antenna to the coordinates determined in section 4.2. We checked the data span to ensure that no cycle slip occurs during the whole observation period. Then, we fixed the carrier phase ambiguity parameter to an integer with the first epoch observations, so that the variation of the double differenced carrier phase residuals is mainly contributed by the antenna PCV variation. Then the GNSS observations are corrected by the PCV compensation algorithm described in section 2 and the cumulative probability function (CDF) of the RTK carrier phase residuals before and after PCV compensation is presented in Figure 16. The figure indicates that the correction of PCV can reduce the carrier phase residuals, while the performance on the two scenarios is different. The improvement for the weight 0.4 case is more significant than weight 0.8 case. After correction,

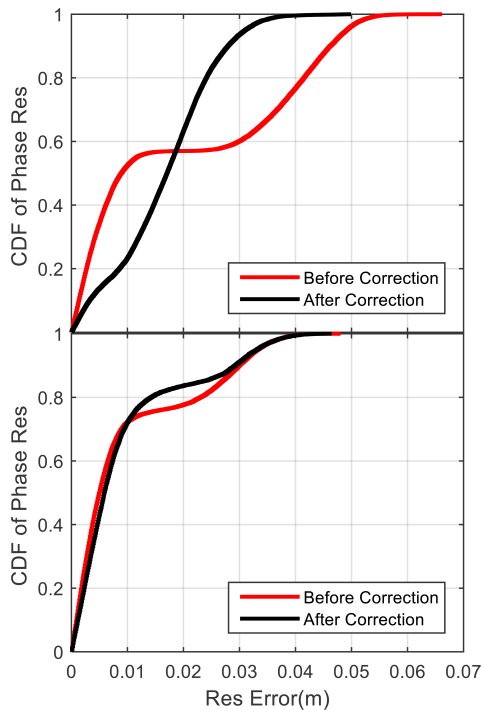


FIGURE 16. CDF of the RTK carrier phase residuals before and after the correction of PCV. (Upper: Weight 0.4 Lower: Weight 0.8).

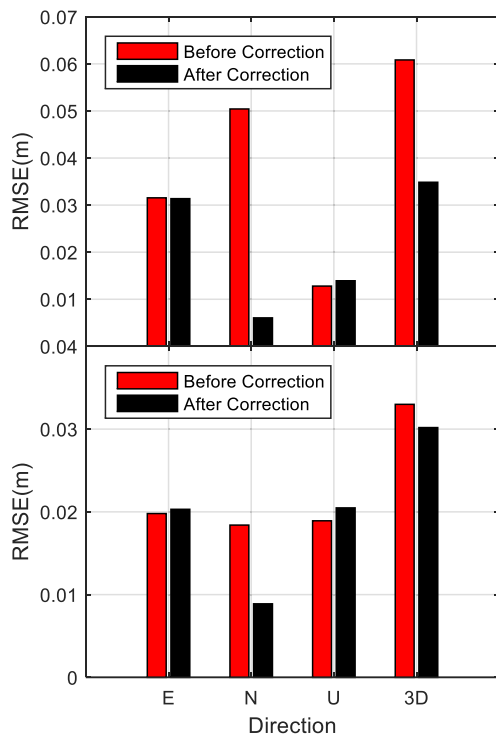


FIGURE 17. The RTK Positioning RMSE improvement after PCV correction (Upper: Weight 0.4 Lower: Weight 0.8).

the probability of carrier phase residuals small than 4 cm achieves 99.73% and 99.92%.

We further examined the RTK positioning accuracy by comparing the positioning results with the reference APC

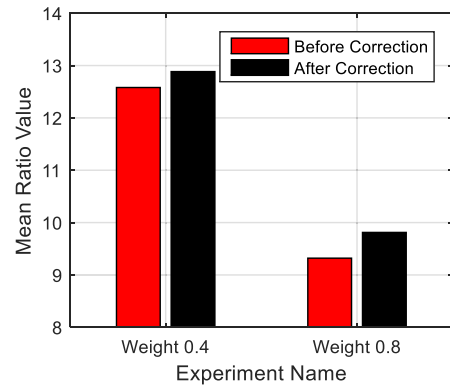


FIGURE 18. The ratio value improvement in RTK data processing after applying for PCV compensation.

position of the anti-jamming antenna. The root mean squared error (RMSE) of the RTK positioning error is illustrated in Figure 17. In the RTK positioning accuracy evaluation, we performs the standard RTK with the observations collected from the anti-jamming antenna and compares the positioning results with the reference value. The figure indicates that applying PCV correction can improve the RTK Positioning accuracy in both scenarios. The 3D positioning accuracy improvement for weight 0.4 and 0.8 cases reaches 42.7% and 9.3% respectively. After correction, both examples achieve 3D RTK accuracy better than 4 cm. More specifically, the positioning accuracy improvement is the most dramatically in north to south direction which is related to the arrangement of the antenna elements.

Another benefit of the PCV correction is improving the reliability of RTK ambiguity resolution. In GNSS RTK data processing, the reliability of RTK ambiguity is often measured by the ratio test value [27]. The definition of value can be found in [28]. The larger ratio value means the fixed integer ambiguity is more likely to be true. We also inspected the ratio value of the RTK data processing and the results are presented in Figure 18. The figure indicates that the ratio value increases by 2.4% and 5.3% for the two experiments respectively.

We further tested the computation efficiency of the proposed algorithm. The PCV compensation algorithm is running on a desktop with Intel i3-2310M CPU whose main frequency 2.10 GHz. We computed 2792 samples, which takes only 0.279 seconds, which computing each PCV correction takes only 0.074 ms. Considering the system overhead, our algorithm is eligible to run in an embedded MCU with several tens of MHz main frequency in real time.

D. DISCUSSIONS

The experiment has demonstrated that the proposed PCV compensation algorithm is effective, but the improvement is not as dramatic as expected. The reason is multi-folds. For example, the inter-channel hardware biases may present in the anti-jamming module, which introduces extra biases in the real data test. The hardware biases between different elements have been captured with the network analyzer, but it varies

over time. The synchronization accuracy of the A/D converter is another factor. The synthetic signals from multiple signals should be very accurate to keep a highly accurate alignment of the carrier phase from different elements, while it is difficult to implement. The general anti-jamming antenna ignored the carrier phase alignment requirement, which increases the uncertainty of PCV variation. Another factor is the mutual coupling of the antenna array. The modeling of the PCV variation assumes all the elements are ideal, but this is not the case in real data tests. Overall, we attempt to solve the PCV compensation problem in the anti-jamming antenna, but there are still many things worth looking into.

V. CONCLUSION

This study proposed a real-time phase center variation compensation algorithm for the anti-jamming antennas to enable high precision GNSS positioning. The phase center variation is the bottleneck problem of applying the anti-jamming antennas in high precision applications. In this study, we modeled the phase center of the nulling antenna array by an instantaneous phase center (IPC) estimation algorithm. After the IPC is estimated, the PCV caused by the power inversion (PI) beamforming algorithm can be compensated in real-time. The impact of PCV was examined with both simulation and real-data test. The simulation results indicate that the PCV caused by the PI algorithm reaches 1 cycle at maximum and the PCV presence discontinuity near the direction of the jamming signals. The performance of the PCV compensation algorithm is also tested with two groups of short baseline RTK experiments with different element weights. In the experiment, the APC of the antenna array is firstly determined and the PCV bias is isolated by fixing the position and carrier phase ambiguity parameters. The test results indicated that the carrier phase residuals becomes smaller after applying for PCV compensation. Consequently, the RTK positioning accuracy is improved by 42.3% and 9.7% respectively. After PCV compensation, the 3D RTK positioning accuracy achieves better than 4 cm. The results also indicate PCV compensation also improved the reliability of RTK ambiguity resolution, which improved the mean ratio value by 2.4% and 5.3% respectively for the two experiments. Meanwhile, this research also concludes that there still are several challenges in PCV compensation of anti-jamming GNSS antenna and hopefully the performance can be further improved with better antenna design.

REFERENCES

- [1] B. W. Parkinson, "Assured PNT for our future: PTA. Actions necessary to reduce vulnerability and ensure availability," *GPS World*, vol. 14, pp. 1–10, Apr. 2014.
- [2] G. X. Gao, M. Sgammini, M. Lu, and N. Kubo, "Protecting GNSS receivers from jamming and interference," *Proc. IEEE*, vol. 104, no. 6, pp. 1327–1338, Jun. 2016.
- [3] U. S. Kim, "Analysis of carrier phase and group delay biases introduced by CRPA hardware," in *Proc. ION GNSS*, 2005, pp. 635–642.
- [4] H. Zhao, B. Lian, and J. Feng, "Adaptive beamforming and phase bias compensation for GNSS receiver," *J. Syst. Eng. Electron.*, vol. 26, no. 1, pp. 10–18, Feb. 2015.
- [5] A. Konovaltsev, L. Greda, M. V. T. Heckler, and A. Hornbostel, "Phase centre variations in adaptive GNSS antenna arrays," in *Proc. 4th ESA Workshop Satell. Navigat. Equip. Technol.*, 2008, pp. 1–18.
- [6] D. Wang, J. Li, X. Zhou, and S. Wu, "Phase center correction for GNSS adaptive anti-jamming antenna array," *Trans. Beijing Inst. Technol.*, vol. 37, pp. 325–330, Feb. 2017.
- [7] X. Chen, G. Fu, S. Gong, H. Liu, and Y. Yan, "Study on measurement of phase center of array antenna," *J. Microw.*, vol. 27, no. 1, pp. 36–39, 2011.
- [8] I. J. Gupta, I. M. Weiss, and A. W. Morrison, "Desired features of adaptive antenna arrays for GNSS receivers," *Proc. IEEE*, vol. 104, no. 6, pp. 1195–1206, Jun. 2016.
- [9] B. Liu, "Study of GNSS antenna phase center and anti-jam technology," M.S. thesis, School Electron. Eng., Univ. Electron. Sci. Technol. China, Chengdu, China, 2016.
- [10] L. Li, F. Wang, D. Li, B. Li, and H. Chen, "Phase centre performance evaluation for GNSS adaptive array," *Electron. Lett.*, vol. 52, no. 14, pp. 1259–1261, Jul. 2016.
- [11] L. Cao, X. An, G. Hong, and B. Guo, "Analysis of measurement biases induced by adaptive antenna arrays for GNSS receivers," in *Proc. 12th Int. Conf. Natural Comput., Fuzzy Syst. Knowl. Discovery*, Aug. 2016, pp. 1863–1867.
- [12] F. Chen, "Interference mitigation and measurement biases compensation for GNSS antenna array receivers," Ph.D. dissertation, Inf. Commun. Eng. Graduate School, Nat. Univ. Defence Technol., Changsha, China, 2017.
- [13] T. Marathe, S. Daneshmand, and G. Lachapelle, "Assessment of measurement distortions in GNSS antenna array space-time processing," *Int. J. Antennas Propag.*, vol. 2016, pp. 1–17, 2016.
- [14] H. Xu, X. Cui, and M. Lu, "Effects of power inversion spatial only adaptive array on GNSS receiver measurements," *Tsinghua Sci. Technol.*, vol. 23, no. 2, pp. 172–183, Apr. 2018.
- [15] W. Kunysz, "Antenna phase center effects and measurements in GNSS ranging applications," in *Proc. 14th Int. Symp. Antenna Technol. Appl. Electromagn. Amer. Electromagn. Conf.*, Jul. 2010, pp. 1–4.
- [16] A. I. El-Hattab, "Influence of GPS antenna phase center variation on precise positioning," *NRIAG J. Astron. Geophys.*, vol. 2, no. 2, pp. 272–277, Dec. 2013.
- [17] R. Schmid, M. Rothacher, D. Thaller, and P. Steigenberger, "Absolute phase center corrections of satellite and receiver antennas," *GPS Solutions*, vol. 9, no. 4, pp. 283–293, Nov. 2005.
- [18] B. Görres, J. Campbell, M. Becker, and M. Siemes, "Absolute calibration of GPS antennas: Laboratory results and comparison with field and robot techniques," *GPS Solutions*, vol. 10, no. 2, pp. 136–145, May 2006.
- [19] R. M. Shubair and W. Jessmi, "Performance analysis of SMI adaptive beamforming arrays for smart antenna systems," in *Proc. IEEE Antennas Propag. Soc. Int. Symp.*, Jul. 2005, pp. 311–314.
- [20] H. Nan and H. Yulin, "Research and comparison of anti-jamming performances of LMS and LCMV algorithm based on MATLAB simulation," in *Proc. IEEE 10th Int. Conf. Electron. Meas. Instrum.*, Aug. 2011, pp. 98–101.
- [21] D. N. Patel, B. J. Makwana, and P. B. Parmar, "Comparative analysis of adaptive beamforming algorithm LMS, SMI and RLS for ULA smart antenna," in *Proc. Int. Conf. Commun. Signal Process. (ICCS)*, Apr. 2016, pp. 1029–1033.
- [22] J. Xu, N. Xu, J. Hua, and C. Song, "Comprehensive performance analysis of power-inversion algorithm used in GPS adaptive arrays," in *Proc. Int. Conf. Microw. Millim. Wave Technol.*, Chengdu, China, May 2010, pp. 1138–1141.
- [23] Y. Tian, X. Yi, and P. Li, "Performance and simulation of adaptive anti-jamming based on power inversion algorithm," *Electron. Inf. Warfare Technol.*, vol. 31, no. 5, pp. 66–70, 2016.
- [24] Y. Zhu, B. Li, J. Liu, and K. Cao, "DOA estimation analysis for satellite navigation jamming," *J. Projectiles Rockets Missiles Guid.*, vol. 36, pp. 131–135 and 146, Feb. 2016.
- [25] L. Wang, Y. Feng, and C. Wang, "Real-time assessment of GNSS observation noise with single receivers," *J. Global Positioning Syst.*, vol. 12, pp. 73–82, 2013.
- [26] P. Misra and P. Enge, *Global Positioning System: Signals, Measurements and Performance*, 2nd ed. Lincoln, MA, USA: Ganga-Jamuna Press, 2006.
- [27] L. Wang, S. Verhagen, and Y. Feng, "Ambiguity acceptance testing: A comparison of the ratio test and difference test," in *Proc. China Satell. Navigat. Conf. (CSNC)*, Nanjing, China, 2014, pp. 313–330.
- [28] L. Wang, Y. Feng, and J. Guo, "Reliability control of single-epoch RTK ambiguity resolution," *GPS Solutions*, vol. 21, no. 2, pp. 591–604, Apr. 2017.

•••